To cite this article: CHEN H, ZHOU R P, FAN H, et al. Analytical and experimental research on impact load during rapid engagement of gas turbine [J/OL]. Chinese Journal of Ship Research, 2022, 17(2). http://www.ship-research.com/en/article/doi/10.19693/j.issn.1673-3185.02341.

DOI: 10.19693/j.issn.1673-3185. 02341

Analytical and experimental research on impact load during rapid engagement of gas turbine

CHEN Hao[1], *ZHOU Ruiping*[*1], *FAN Hong*[1], *LEI Junsong*[1], *ZHOU Shaowei*[2]

1 School of Naval Architecture, Ocean and Energy Power Engineering, Wuhan University of Technology, Wuhan 430063, China

2 China Ship Development and Design Center, Wuhan 430064, China

Abstract: [**Objectives**] This paper proposes a theoretical calculation method for obtaining the impact load and dynamic response of shafting during the rapid engagement of a combined gas turbine and gas turbine (COGAG) power plant. [**Methods**] According to the mechanical relationships between various components in the meshing process of a synchro-self-shifting (SSS) clutch, a dynamic analysis model of the clutch is established, and the dynamic simulation and bench test during the rapid engagement of COGAG are carried out. [**Results**] The simulation results show that when the damping dashpot functions, an obvious torque impact appears in the helical spline of the clutch, which can result in a strong dynamic response on the shafting. It is also found that the relative position of the ratchet and pawl is random, which can make the peak of the torque impact and the dynamic response of the shafting fluctuate within a certain range. Through a bench test, the accuracy of the impact load calculation method is verified, and in comparison with the theoretical result, the deviation of its maximum and minimum torque response amplitudes from the theoretically calculated values is 3.56% and 8.86%, respectively. [**Conclusions**] This paper studies torque impact during the rapid engagement of gas turbines, and the result can provide a reference for the safety evaluation of COGAG power plants.

Key words: combined gas turbine and gas turbine (COGAG) power plant; rapid engagement; synchro-self-shifting (SSS) clutch; impact load

CLC number: U664.16

0 Introduction

A combined gas turbine and gas turbine (COGAG) power plant generally uses a single gas turbine for propulsion under cruising conditions and two engaged gas turbines for propulsion under accelerating conditions. In addition, the engagement of gas turbines requires a steady variation of speeds and loads. For this reason, it is often necessary to first synchronize the rotation of the working gas turbine and the engaging one at a low speed and then gradually transfer loads after stable meshing of a synchro-self-shifting (SSS) clutch. As a result, the whole process takes a long time. In some emergency cases, for example, when a warship encounters the enemy and needs the rapid engagement of gas turbines for power increase, the rapid increase in load will produce an obvious torque impact which acts on the propulsion shafting. As this impact load may affect the shafting connected before and after the clutch adversely, it is necessary to study its occurrence mechanisms and influencing factors.

Received: 2021－04－04 **Accepted**: 2021－05－20

Supported by: National Science and Technology Major Project (2017-IV-0006-0043); National Natural Science Foundation of China (51839005)

Authors: CHEN Hao, male, born in 1993, Ph.D. candidate. Research interest: performance analysis and vibration-noise control of ship power plants. E-mail: 1361700535@qq.com

ZHOU Ruiping, male, born in 1964, Ph.D., professor, doctoral supervisor. Research interest: performance analysis and vibration-noise control of ship power plants. E-mail: rpzhouwhut@126.com

***Corresponding author**: ZHOU Ruiping

At present, scholars both in China and abroad have studied the meshing dynamics of SSS clutches extensively. By establishing mechanical models, Jiang et al. [1], Jiang [2], Jiang [3], and Tian et al. [4] analyzed the meshing of a SSS clutch through simulation. Zhang et al. [5] and Zhang et al. [6] calculated the motion of a SSS clutch by three-dimensional models and multi-body dynamic simulation software. These studies mainly analyzed the influence of meshing time, relative speeds, and damping apertures of SSS clutches through simulation. In terms of test research, Wei [7] analyzed the meshing of a SSS clutch under no-load conditions. By setting up a test bench with motors as prime movers and loads, Zhang et al. [8-9] analyzed the operational performance of SSS clutches during the de-meshing and load transfer. In addition, by setting up a test bench of a combined diesel or gas (CODOG) power plant with gas turbines and diesel engines as prime movers, Tian et al. [10] studied the state of SSS clutches under switching conditions and obtained rich measured data. Luneburg et al. [11] studied impact loads during the engagement of single-shaft gas turbines. However, as some parameters in their dynamic model are defined implicitly, it is difficult to find solutions and then popularize the model. Chen et al. [12] analyzed impact loads and shafting responses during the meshing of a SSS clutch by ADAMS, but they failed to verify the theoretical method experimentally.

In conclusion, global studies on occurrence mechanisms and influencing factors of torque impacts during the rapid engagement of COGAG power plants are not in-depth enough and lack of corresponding test verification. Therefore, based on the dynamic analysis of SSS clutch meshing, this paper studies the dynamic state of SSS clutches during the rapid engagement of gas turbines and establishes a test bench for verification analysis.

1 Working principle and dynamic analysis of a SSS clutch

1.1 Working principle of a SSS clutch

A SSS clutch can mesh and demesh automatically through the speed difference between driving and driven ends, and it is composed of driving, driven, and middle members. For a relay SSS clutch with high load-bearing capacity, it is also equipped with a relay. Fig. 1 illustrates the structure and working principle of a SSS clutch.

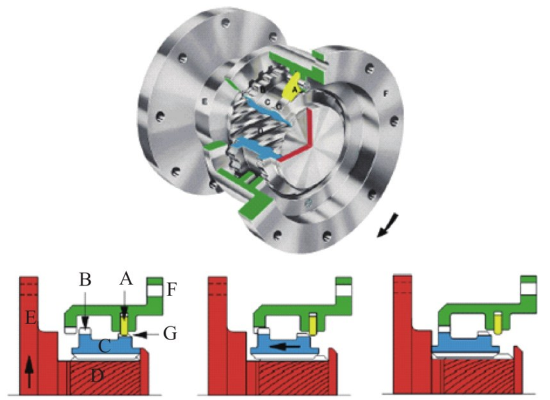

(a) Meshing initiation (b) During meshing (c) Meshing completion

A-Pawl;B-Meshing gear; C-Middle member; D-Helical spline shaft; E-Driving member; F-Driven member; G-Ratcher

Fig. 1 Mechanical structure and basic principle of a SSS clutch

1.2 Dynamic analysis of SSS clutch meshing

1) Force analysis of driving member.

In the initial stage of meshing, the driving member will be subjected to external moment $M_{\rm in}$, circumferential moment $M_{\rm hr}$ caused by the tangential component of tooth-surface pressure on a helical tooth, circumferential moment $M_{\rm fr}$ caused by the tangential component of tooth-surface friction force, axial component $F_{\rm ha}$ of tooth-surface pressure, axial component $F_{\rm fa}$ of tooth-surface friction force, and axial force $F_{\rm b1}$ on the end face restricting axial movement. In addition, the middle member will bear recoil resistance under the action of the damping dashpot when it is close to the end face of the helical spline shaft, so as to avoid a strong rigid collision. As a result, the driving member will bear reaction force $F_{\rm R}$ of the recoil resistance.

The dynamic equation of the driving member can be expressed as follows:

$$\begin{cases} M_{\rm in} - M_{\rm hr} - M_{\rm fr} = J_{\rm in} \cdot \dfrac{{\rm d}\omega_{\rm in}}{{\rm d}t} \\ F_{\rm fa} - F_{\rm ha} - F_{\rm b1} - F_{\rm R} = 0 \end{cases} \tag{1}$$

where $J_{\rm in}$ is the moment of inertia of the driving member; $\omega_{\rm in}$ is the angular velocity of the driving member; t represents the time.

$F_{\rm R}$ can be expressed empirically as follows:

$$F_{\rm R} = \begin{cases} c \cdot \left(\dfrac{D_{\rm t}}{2\tan\beta}\right)^2 \cdot (\omega_{\rm in} - \omega_{\rm s})^2, & \forall x_{\rm s} \geqslant L_{\rm R} \\ 0, & \forall x_{\rm s} < L_{\rm R} \end{cases} \tag{2}$$

where c is the damping coefficient; $D_{\rm t}$ is the reference diameter of the helical spline; β is the helix angle of the helical spline; $\omega_{\rm s}$ is the angular velocity of the middle member, and the difference between $\omega_{\rm in}$ and $\omega_{\rm s}$ is the axial velocity of the middle member; $x_{\rm s}$ is the axial sliding distance of the middle member; L_R is the sliding distance of the middle member when the damping dashpot starts to produce recoil force.

In the equation,

$$c = \frac{\rho A_c^3}{2\mu^2 A^2} \tag{3}$$

where ρ is the density of lubricating oil; A_c is the cross-sectional area of the damping dashpot; μ is the flow coefficient of the damping oil hole; A is the cross-sectional area of the damping oil hole.

2) Force analysis of middle member.

In the initial stage of meshing, the middle member will be subjected to circumferential moment M_p and axial friction force F_{fp} caused by tooth-surface pressure of the ratchet and pawl, as well as reaction forces F_{ha} and F_{fa} and reaction moments M_{hr} and M_{fr} from the driving member. During the meshing, the ratchet and the pawl will demesh slowly, and the main gear and the gear ring will mesh gradually. After the ratchet and the pawl are separated, the middle member will also be subjected to circumferential moment M_g and axial friction force F_{fg} produced by the main gear, and it will bear recoil damping force F_R when the meshing is almost completed.

The dynamic equation of the middle member can be expressed as follows:

$$\begin{cases} M_{hr} + M_{fr} - (M_p + M_g) = J_s \cdot \dfrac{d\omega_s}{dt} \\ F_{ha} - F_{fa} - (F_{fp} + F_{fg}) - F_R = m_s \cdot \dfrac{dv_s}{dt} \end{cases} \tag{4}$$

where J_s is the moment of inertia of the middle member; m_s is the mass of the middle member; v_s is the axial velocity of the middle member.

In the equation,

$$v_s = \begin{cases} \dfrac{D_t}{2\tan\beta}(\omega_{in} - \omega_s), & \forall \omega_{in} \geqslant \omega_s \\ 0, & \forall \omega_{in} < \omega_s \end{cases} \tag{5}$$

3) Force analysis of driven member.

During the meshing, the driven member will be subjected to driven-end moment M_{ex}, reaction moments M_p and M_g and reaction forces F_{fp} and F_{fg} from the middle member, and force F_{b2} that restricts the axial motion of the driven member.

The dynamic equation of the driven member can be expressed as follows:

$$\begin{cases} M_g + M_p - M_{ex} = J_{out} \dfrac{d\omega_{out}}{dt} \\ F_{b2} - (F_{fp} + F_{fg}) = 0 \end{cases} \tag{6}$$

where J_{out} is the moment of inertia of the driven member; ω_{out} is the angular velocity of the driven member.

As the driven member always constrains the circumferential rotation of the middle member during the meshing, the following equation is obtained.

$$\omega_s = \omega_{out} \tag{7}$$

2 Occurrence mechanism of load during rapid engagement and disengagement of two gas turbines

2.1 External conditions of SSS clutch meshing

The driving moment M_{in} of the driving end of a SSS clutch is determined by the output torque of the gas turbine connected to the clutch, while the external torque M_{ex} of the driven end is determined by the overall motion state of the shafting of a COGAG power plant. The shafting of a COGAG power plant generally consists of a propeller, a gearbox, a SSS clutch, gas turbines, and relevant connecting shafts, as shown in Fig. 2.

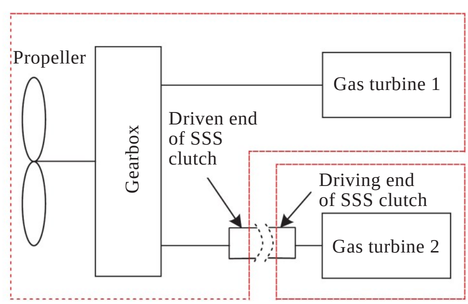

Fig. 2 Diagram of shafting structure

In Fig. 2, the shafting is divided into two parts before and after the driven member of the SSS clutch. The dynamic equation of the rear-end shafting (connected with the gearbox) of the driven member is expressed as follows:

$$(M_{ex} + M_T) \cdot i - M_{pro} = \tilde{J} \cdot \frac{d\omega_{out}}{dt} \tag{8}$$

where M_T is the output torque of the engaged gas turbine in operation; i is the reduction ratio of the gearbox; M_{pro} is the resistance moment of the propeller; $\tilde{J}$ is the equivalent moment of inertia of the rear-end shafting.

In the equation,

$$\tilde{J} = i^2 \cdot J_{front} + J_{rear} \tag{9}$$

where J_{front} is the moment of inertia of the undecelerated component of the shafting (including the pinion of the gearbox); J_{rear} is the moment of inertia of the decelerated component of the shafting (including the gearwheel of the gearbox).

M_{pro} can be calculated by the following equation:

$$M_{\rm pro} = K_Q \rho_{\rm w} n_{\rm p}^2 D^5 \tag{10}$$

where K_Q is the torque coefficient of the propeller; $\rho_{\rm w}$ is the density of seawater; $n_{\rm p}$ is the calculated speed of the propeller; D is the diameter of the propeller.

Based on Eq. (8), the equation of the moment of momentum in Eq. (6) can be deduced as follows:

$$M_{\rm r} - \left(J_{\rm out} + \frac{\tilde{J}}{i}\right)\frac{{\rm d}\omega_{\rm s}}{{\rm d}t} = \frac{M_{\rm pro} - i \cdot M_{\rm T}}{i} \tag{11}$$

where $M_{\rm r}$ is the equivalent restricting moment, which is $M_{\rm p}$ before ratchet-pawl separation and $M_{\rm g}$ after ratchet-pawl separation.

2.2 Dynamic calculation of SSS clutch meshing

During the meshing of a SSS clutch, the speed and position of each member determine the meshing state of the SSS clutch. The integral equations are as follows:

For the driving member,

$$\varphi_{\rm in} = \int \omega_{\rm in} {\rm d}t \tag{12}$$

For the middle member,

$$\begin{cases} \varphi_{\rm s} = \int \omega_{\rm s} {\rm d}t \\ x_{\rm s} = \int v_{\rm s} {\rm d}t \end{cases} \tag{13}$$

For the driven member,

$$\varphi_{\rm out} = \int \omega_{\rm out} {\rm d}t \tag{14}$$

In Eq. (12)-Eq. (14), $\varphi_{\rm in}$, $\varphi_{\rm s}$, $\varphi_{\rm out}$ are rotation angles of driving, middle, and driven members, respectively.

The dynamic matrix equation of SSS clutch meshing is as follows:

$$\begin{bmatrix} A_1 & 0 & J_{\rm in} & 0 \\ A_1 & -1 & 0 & -J_{\rm s} \\ A_2 & A_3 & -A_4 & A_4 \\ 0 & 1 & 0 & A_5 \end{bmatrix} \cdot \begin{bmatrix} M_{\rm hr} \\ M_{\rm r} \\ \frac{{\rm d}\omega_{\rm in}}{{\rm d}t} \\ \frac{{\rm d}\omega_{\rm s}}{{\rm d}t} \end{bmatrix} = \begin{bmatrix} M_{\rm in} \\ 0 \\ F_{\rm R} \\ C_1 \end{bmatrix} \tag{15}$$

where $A_1 = 1 + \dfrac{\tan\beta \cdot f_{\rm h}}{\cos\alpha_1}$ and $f_{\rm h}$ is the friction coefficient of the helical tooth surface; α_1 is the pressure angle of the helical spline tooth surface; $A_2 = \dfrac{2(\tan\beta\cos\alpha_1 - f_{\rm h})}{D_{\rm t} \cdot \cos\alpha_1}$; $A_3 = \begin{cases} -\dfrac{2f_{\rm p}}{D_{\rm p} \cdot \cos\alpha_2}, \ \forall x_{\rm s} < L_{\rm p} \\ -\dfrac{2f_{\rm g}}{D_{\rm g} \cdot \cos\alpha_3}, \ \forall x_{\rm s} \geqslant L_{\rm p} \end{cases}$,

where $f_{\rm p}$ and $f_{\rm g}$ are friction coefficients of ratchet-pawl and main gear-gear ring contact surfaces, respectively; $D_{\rm p}$ and $D_{\rm g}$ are the diameter of the ratchet-pawl contact point and the pitch diameter of the main gear, respectively; α_2 and α_3 are equivalent pressure angles of the ratchet-pawl contact surface and the main gear, respectively; $L_{\rm p}$ is the sliding distance of the middle member when the ratchet and pawl are separated; $A_4 = \dfrac{m_{\rm s} \cdot D_{\rm t}}{2\tan\beta}$; $A_5 = -\left(J_{\rm out} + \dfrac{\tilde{J}}{i}\right)$; $C_1 = \dfrac{M_{\rm pro} - i \cdot M_{\rm T}}{i}$.

Before the engagement of a COGAG power plant, it is assumed that one gas turbine (hereinafter referred to as the working machine) drives the shafting to run at a speed of n_0. After an engagement instruction is issued, the other gas turbine (hereinafter referred to as the engaging machine) will engage with the working one. Before the speed of the power turbine of the engaging machine reaches n_0, the driven end of the SSS clutch will rotate at a speed of n_0. After that, the driving member of the clutch will drive the middle member to slide under the drive of the gas turbine. Specifically, the clutch operates according to the dynamic relationship described in Eq. (15) until the meshing is completed. In this paper, simulation analysis starts when the speed of the engaging machine reaches n_0. As the meshing takes less than 1 s, it is assumed that gas turbines will output power with constant torque during the meshing. Generally, in order to achieve a smooth system operation, the engaging machine will drive the driving end to accelerate continuously with low torque until the meshing is done. However, under rapid engagement, the engaging machine will drive the clutch to mesh directly, with output torque equivalent to that of the working machine, so as to shorten the engagement time and raise the output power of the power plant in a short time.

In view of the two-machine engagement shafting in the test bench in Fig. 3, this paper establishes a model in Matlab and sets the torques of the working and engaging machines to 12 N·m and 6 N·m, respectively. Fig. 4 and Fig. 5 illustrate the motion of the middle member and the torque of the helical spline during SSS clutch meshing, respectively. From Fig. 4, it can be seen that when the middle member slides to the position where the recoil damping force works at t_1, its axial sliding speed slows down. Then, the member slides gradually to the meshing completion position and completes the meshing at t_2. Fig. 5 shows that an obvious torque impact occurs on the helical tooth at t_1, with an amplitude of 230.04 N·m.

At the moment of the torque impact, although the clutch meshing has not yet been completed, the

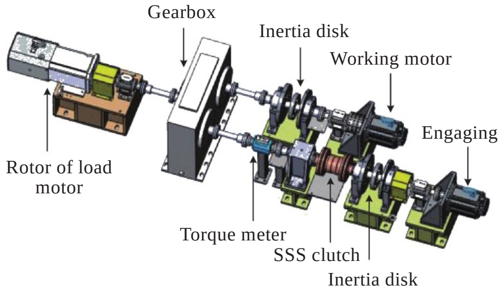

Fig. 3 Diagram of the test bench

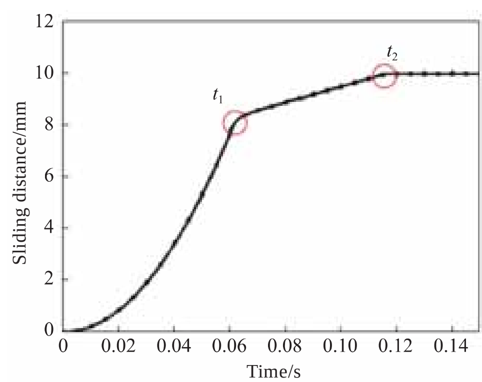

Fig. 4 Sliding distance of the middle member

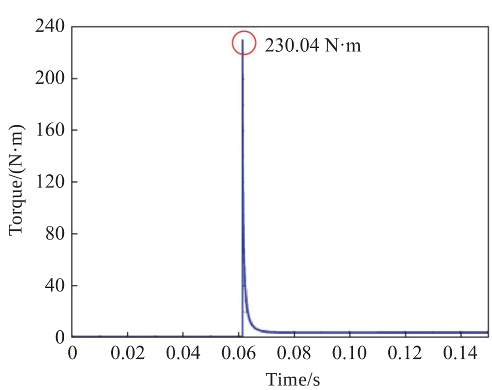

Fig. 5 Torque on the spiral spline

torque impact comes from the helical tooth and will act on the shafting connected with the driving and driven ends simultaneously. Differential equations of the shafting at the driving and driven ends are as follows:

$$\boldsymbol{J}_{\rm in}\cdot\ddot{\theta}+\boldsymbol{C}_{\rm in}\cdot\dot{\theta}+\boldsymbol{K}_{\rm in}\cdot\theta=\boldsymbol{T}_{\rm s}(t) \tag{16}$$

$$\boldsymbol{J}_{\rm ex}\cdot\ddot{\theta}'+\boldsymbol{C}_{\rm ex}\cdot\dot{\theta}'+\boldsymbol{K}_{\rm ex}\cdot\theta'=-\boldsymbol{T}_{\rm s}(t) \tag{17}$$

where $\boldsymbol{J}_{\rm in}$, $\boldsymbol{C}_{\rm in}$, $\boldsymbol{K}_{\rm in}$ are inertia, damping, and stiffness matrixes of the shafting at the driving end, respectively; $\boldsymbol{J}_{\rm ex}$, $\boldsymbol{C}_{\rm ex}$, $\boldsymbol{K}_{\rm ex}$ are inertia, damping, and stiffness matrixes of the shafting at the driven end, respectively; $\theta,\dot{\theta},\ddot{\theta}$ are angular displacement, velocity, and acceleration vectors of the shafting at the driving end, respectively; θ', $\dot{\theta}'$,$\ddot{\theta}'$ are angular displacement, velocity, and acceleration vectors of the shafting at the driven end, respectively; $\boldsymbol{T}_{\rm s}(t)$ is the vector formed by impact loads during the engagement.

Parameters of dynamic models of the shafting are listed in Table 1 and Table 2, respectively.

Table 1 Parameters of the driving end

Component	Inertia/ (kg·cm^2)	Stiffness /(kN·m·rad^{-1})	Internal damping coefficient
Rotor of engaging machine	15 825.06	78.20	0.064
Inertia disk	23 078.54	326.29	0.064
Driving part of clutch	9 954	–	–

Table 2 Parameters of the driven end

Component	Inertia/ (kg·cm^2)	Stiffness /(kN·m·rad^{-1})	Internal damping coefficient
Driven part of clutch	31 377.86	46.45	0.064
Pinion	8 616.855	–	–
Gearwheel	245 749.7	49.35	0.064
Rotor of load machine	55 446.19	–	–
Pinion (branch 1)	6 218.73	71.79	0.064
Inertia disk (branch 1)	26 697.27	78.20	0.064
Rotor of working machine (branch 1)	15 825.06	–	–

A lumped parameter model of the shafting is established according to the modeling principle of a chained system, and then the time-domain integration of Eq. (16) and Eq. (17) is carried out through the Newmark method. On this basis, responses of the shafting at the driving and driven ends under torque impacts are obtained, as shown in Fig. 6 and Fig. 7. From the figures, it is found that under the impact torque, rotors at both driving and driven ends generate obvious torque responses, and their amplitudes are 59.31 N·m and 12.54 N·m, respectively, reaching 237.34% and 50.16% of the rated torque, respectively (motors of the test bench in this paper have a rated torque of 25 N·m).

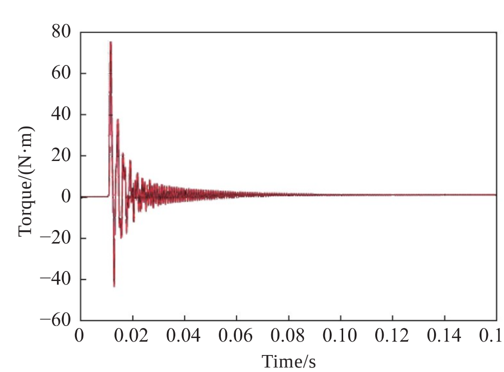

Fig. 6 Torque response of the driving end

2.3 Influence of relative position of ratchet and pawl on torque impact

In the above simulation of gas turbine engagement, it is assumed that the ratchet and the pawl of

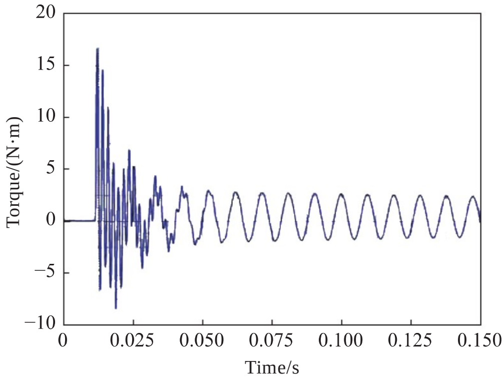

Fig. 7 Torque response of the driven end

the SSS clutch are right in the meshing position when the driving end speed exceeds the driven-end speed. However, in the actual operation, a certain angle between the ratchet and the pawl will appear at this moment. In other words, the driving end needs to accelerate and rotate at an angle of φ_r relative to the driven end for ratchet-pawl meshing. Specifically, the maximum of φ_r is obtained by

$$\varphi_{r\max} = \frac{2\pi}{b \cdot z_p} \tag{18}$$

where b is the number of pawls, and z_p is that of ratchet teeth.

It is assumed that the initial relative angular velocity of the ratchet and pawl is ω_r when they are in contact, and then the maximum of ω_r corresponding to $\varphi_{r\max}$ is given by

$$\omega_{r\max} = \sqrt{\frac{4\pi \cdot M_{in}}{b \cdot z_p \cdot J_{in}}} \tag{19}$$

Generally, ω_r is between 0 and $\omega_{r\max}$ when the driving end starts to mesh, and its value may affect the torque impact during the meshing. Fig. 8 shows the impact torque with ω_r at its maximum and minimum. According to the figure, when ω_r increases from 0 to $\omega_{r\max}$, the peak of the impact torque increases from 230.04 N·m to 794.15 N·m, with an improvement of 245.22%.

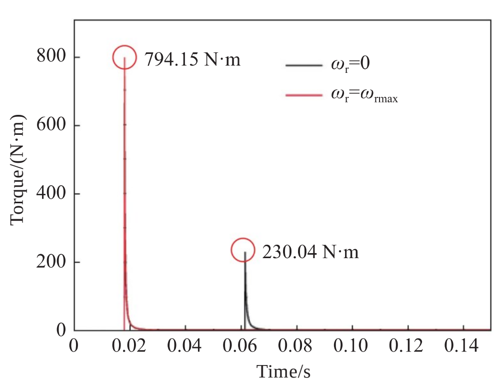

Fig. 8 Torque curve under different ω_r

By applying different output torques M_{in} of the engaging gas turbine and impact torque under ω_r to the shafting, curves of torque response amplitude of the rotor at the driven end can be obtained as M_{in} and ω_r change. As shown in Fig. 9, when M_{in} and ω_r increase, the torque response amplitude of the rotor improves accordingly. For example, when M_{in} equals 6 N·m, the torque response amplitude under ω_r at its maximum is 32.91 N·m, which is 163.07% higher than that under ω_r of 0.

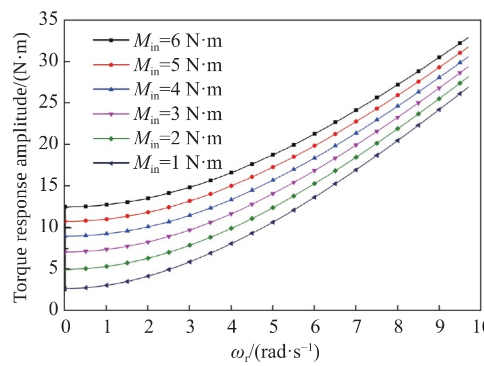

Fig. 9 Torque response amplitudes under different M_{in} and ω_r

Noteworthily, as the relative position of the ratchet and pawl before SSS clutch meshing is random, ω_r is also a random variable as to the system, and this will lead to the randomness of the impact torque and shafting response within a certain range during the engagement.

3 Bench test of engagement

3.1 Test bench

As shown in Fig. 10 and Fig. 11, in the test bench of gas turbine engagement, two drive motors are used to simulate the working characteristics of gas turbines (hereinafter referred to as working and engaging motors), and a load motor is used to simulate those of a propeller. The three motors are connected by an engagement gearbox with a speed ratio of 3∶1. Specifically, a SSS clutch is installed between the engaging motor and the input shaft of the gearbox, and a torque meter is arranged between the driven end of the clutch and the input shaft of the gearbox. Table 3 lists the main equipment parameters of the test bench.

3.2 Test process and data analysis

The control flow of the engagement test is as follows:

1) The output of the working motor is set to 12 N·m, and the corresponding torque of the load motor is set simultaneously.

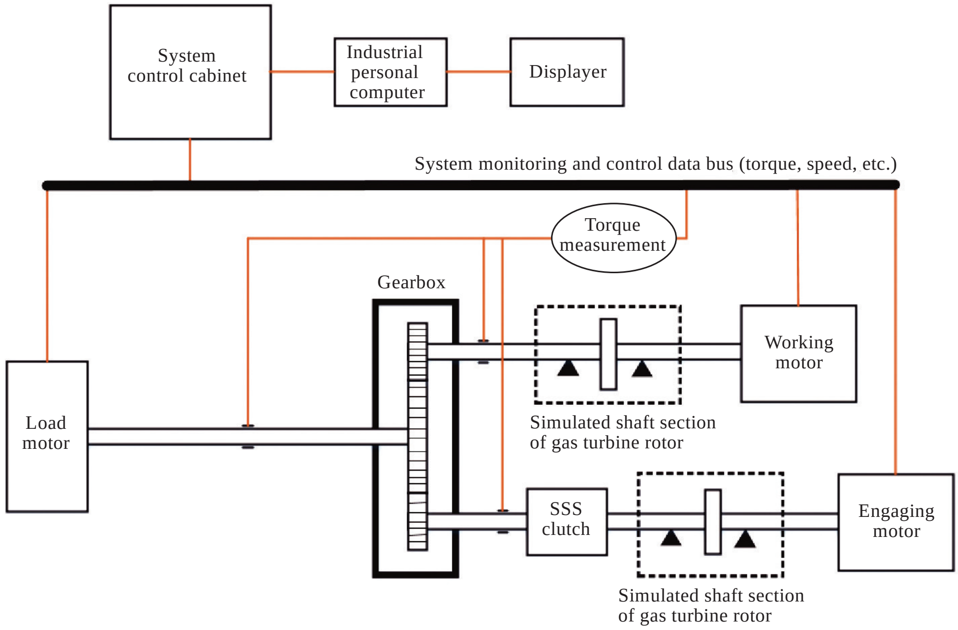

Fig. 10 Schematic diagram of the test bench

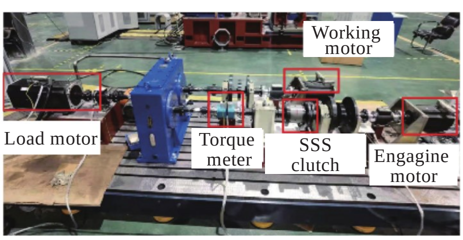

Fig. 11 Equipment layout of the test bench

Table 3 Main parameters of the test bench

Device	Main parameter	Value
Drive motor	Rated power/kW	4
	Maximum speed/(r·min^{-1})	4 000
Load motor	Rated power/kW	10
	Maximum speed/(r·min^{-1})	2 000
SSS clutch	Rated torque/(N·m)	200
Engagement gearbox	Speed ratio	3∶1
Torque meter	Sampling rate/Hz	1 000

2) When the system is stable at a certain speed, the upper computer will issue an engagement instruction, and then the engaging motor starts up with a torque of 6 N·m.

3) As the clutch meshes, the rotational speed of the system gradually increases and tends to be stable, and the engagement is thus completed.

According to the above calculation method and engagement parameters of the test bench, the response amplitude of the shafting under impact loads during the engagement ranges from 12.51 N·m to 32.91 N·m (calculated values).

Fig. 12 shows the transient torque recorded by the torque meter during the test. According to the figure, when the engagement completes, the shafting generates an apparent transient torque response with an amplitude of 19.15 N·m, and the impact lasts about 0.15 s. Repeated tests with the same engagement parameters indicate that the amplitude of this torque fluctuates within a certain range. Fig. 13 shows the torque amplitude in 20 tests. It can be seen that the response of the shafting under torque

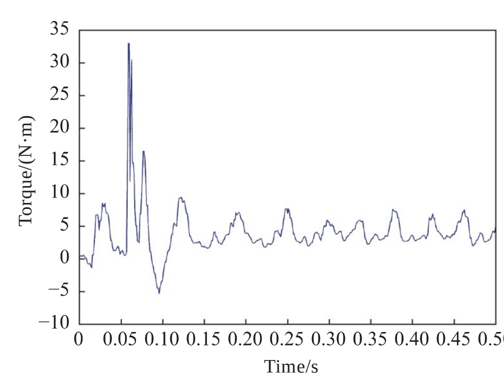

Fig. 12 Transient torque curve of engagement

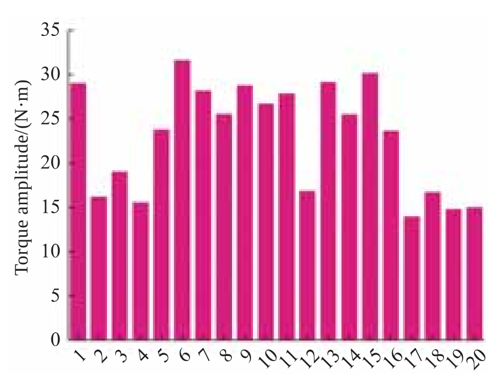

Fig. 13 Torque amplitude in repeated experiments

impacts ranges from 14.07 N·m to 31.74 N·m, and the deviations of its maximum and minimum from the theoretically calculated values are 3.56% and 8.86%, respectively, which verifies the correctness of the theoretical calculation method in this paper.

4 Conclusions

By establishing the dynamic model of a SSS clutch, this paper simulates the rapid engagement of a COGAG power plant, and the following conclusions are drawn:

1) During the rapid engagement, an obvious torque impact will appear on the helical tooth when recoil force is produced in the damping dashpot of the SSS clutch.

2) Under the torque impact, the shafting connected with the driving and driven ends of the clutch will generate obvious dynamic torque responses.

3) Due to the randomness of ratchet-pawl relative positions, the amplitudes of both torque impact and dynamic response of shafting will fluctuate within a certain range during the engagement, which must be considered in safety check.

4) By bench tests, the feasibility of the theoretical calculation method of response amplitude and fluctuation range of shafting under torque impact is verified quantitatively.

This paper studies the occurrence mechanism of impact loads during rapid engagement and disengagement of a COGAG power plant, which provides a reference for the safety evaluation of the COGAG power plant.

References

[1] JIANG D S, TIAN Y, ZHANG Z Y, et al. Mathematical model of S.S.S. based on CODOG system [J]. Journal of Harbin Engineering University, 2001, 22 (4): 22−24, 60 (in Chinese).

[2] JIANG D S. Study on constant damping control characteristic of synchro-self-shifting clutch on combined power plant [C] //2010 Asia–Pacific Power and Energy Engineering Conference (APPEEC). Chengdu, China: IEEE, 2010: 1−4.

[3] JIANG J M. The study of the dynamic simulation for the S.S.S. clutch [D]. Harbin: Harbin Engineering University, 2010 (in Chinese).

[4] TIAN Y, SUN Y F, LU Q C. Simulation of synchronous-self-shifting clutches based on Matlab [J]. Journal of Tsinghua University (Science and Technology), 2004, 44 (2): 255−257, 265 (in Chinese).

[5] ZHANG X Y, LI S Y, JIANG J M, et al. Simulation study on the motion characteristics of S. S. S. clutch in marine power system [J]. Ship Engineering, 2011, 33 (Supp 2): 52−56 (in Chinese).

[6] ZHANG X N, ZHU J H, LI S Y. Research on the engagement process of 3S clutch using ADAMS software [J]. Applied Science and Technology, 2003, 30 (12): 26−28 (in Chinese).

[7] WEI J B. Experiment research of high power marine S. S.S. clutch [J]. Journal of Engineering for Thermal Energy and Power, 1997, 12 (5): 351−353 (in Chinese).

[8] ZHANG X, ZHONG A X, SONG C J, et al. The retrorse experiment research of SSS clutch's capability [J]. Ship Science and Technology, 2010, 32 (8): 148−150, 156 (in Chinese).

[9] ZHANG X, CHEN K X, WANG X Z, et al. Experiment research of synchro-self-shifting clutches incorporation [J]. Ship Science and Technology, 2014, 36 (9): 118−121 (in Chinese).

[10] TIAN Y, NIU Z Y, ZHANG Z Y, et al. Experimental study of the dynamic characteristics of a synchronous self-shifting (SSS) clutch for a combined diesel or gas turbine power plant [J]. Journal of Engineering for Thermal Energy and Power, 2002, 17 (1): 37−40 (in Chinese).

[11] LUNEBURG B, KLOCKE M, KULIG S, et al. Evaluation of impact loads of clutch engaging within single shaft applications for power generation [C] //ASME Turbo Expo 2008: Power for Land, Sea, and Air. Berlin, Germany: ASME, 2008: 1227−1236.

[12] CHEN H, ZHOU R P, LEI J S, et al. Research on dynamic response of propulsion shafting under impact load during engaging process of gas turbine [J]. Journal of Propulsion Technology, 2020, 41 (11): 2509−2517 (in Chinese).

燃机快速并车过程的冲击载荷特性分析及实验研究

陈昊[1],周瑞平[*1],樊红[1],雷俊松[1],周少伟[2]
1 武汉理工大学 船海与能源动力工程学院,湖北 武汉 430063
2 中国舰船研究设计中心,湖北 武汉 430064

摘　要:[目的]为了获取燃燃联合动力(COGAG)装置在快速并车解列过程中的冲击载荷及轴系动态响应,提出一种理论计算方法。[方法]根据同步自动换挡(SSS)离合器啮合过程中各部件的力学关系,建立离合器的动力学分析模型,并开展燃燃联合动力装置并车过程的动力学仿真和台架实验。[结果]仿真结果表明:在阻尼油腔作用的时刻,离合器螺旋花键上产生了明显的扭矩冲击,同时使离合器两端轴系产生了很强的扭矩动态响应;离合器棘轮棘爪位置的随机性将导致扭矩冲击峰值和轴系动态响应在一定范围内波动。台架实验验证了并车冲击载荷计算方法的正确性,其最大和最小扭矩的响应幅值与理论计算偏差分别为3.56% 和8.86%。[结论]对于燃机快速并车过程中的扭矩冲击影响,研究成果可为燃燃联合动力装置的运行安全性评估提供参考。
关键词:燃燃联合动力装置;快速并车;同步自换档离合器;冲击载荷